Received 14 July 2016; revised 1 September 2016; accepted 29 September 2016. Date of current version 24 October 2016.
The review of this paper was arranged by Editor M. Östling.

Digital Object Identifier 10.1109/JEDS.2016.2614915

P-Type Tunnel FETs With Triple Heterojunctions

JUN Z. HUANG[1], PENGYU LONG[1], MICHAEL POVOLOTSKYI[1], GERHARD KLIMECK[1] (Fellow, IEEE), AND MARK J. W. RODWELL[2] (Fellow, IEEE)

1 Network for Computational Nanotechnology and Birck Nanotechnology Center, Purdue University, West Lafayette, IN 47907, USA
2 Department of Electrical and Computer Engineering, University of California at Santa Barbara, Santa Barbara, CA 93106-9560, USA

CORRESPONDING AUTHOR: J. Z. HUANG (e-mail: junhuang1021@gmail.com)

This work was supported in part by the Network for Computational Nanotechnology through the U.S. National Science Foundation under Grant EEC-0228390, Grant EEC-1227110, Grant EEC-0634750, Grant OCI-0438246, Grant OCI-0832623, and Grant OCI-0721680, and in part by the National Science Foundation under Grant 1509394.

ABSTRACT A triple-heterojunction (3HJ) design is employed to improve p-type InAs/GaSb heterojunction (HJ) tunnel FETs. Atomistic quantum transport simulations show, that the added two HJs (AlInAsSb/InAs in the source and GaSb/AlSb in the channel) significantly shorten the tunnel distance and create two resonant states, greatly improving the ON state tunneling probability. Moreover, the source Fermi degeneracy is reduced by the increased source (AlInAsSb) density of states and the OFF state leakage is reduced by the heavier channel (AlSb) hole effective masses. With $V_{DD} = 0.3$V and $I_{OFF} = 1$nA/μm, ballistic I_{ON} of 606μA/μm (492μA/μm) is obtained at 30nm (15nm) channel length, which is comparable to n-type 3HJ counterpart and significantly exceeding p-type silicon MOSFET. Simultaneously, the nonlinear turn on and delayed saturation in the output characteristics are also greatly improved.

INDEX TERMS P-type TFET (pTFET), heterojunction TFET (HJ TFET), triple-heterojunction TFET (3HJ TFET).

I. INTRODUCTION

Steep subthreshold swing (SS) devices, such as tunnel field-effect transistors (TFETs), offer great potential in building future low-power integrated circuits. One problem of TFETs is the low tunneling probability hence low ON state current (I_{ON}). To achieve large I_{ON}, III-V TFET designs have been intensively studied [1]. In particular, InAs/GaSb HJ TFETs can considerably boost I_{ON} due to their broken/staggered band alignments [2]. However, under strong confinement, required for good electrostatic control, the effective band gap and transport effective masses both increase, seriously limiting the tunneling probability. Methods to improve InAs/GaSb HJ n-type TFETs (nTFETs) include strain and doping engineering [3], [4], resonant enhancement [5]–[7], and source/channel heterojunctions [8]–[12]. For p-type TFETs (pTFETs), the problem is more severe, as the optimal source doping density is limited by the small conduction band density of states (DOS) [13]. This leads to a large depletion region in the source and thus, smaller I_{ON} than nTFETs [14]–[16]. Doping and heterojunction engineering in the source [17] have been proposed to mitigate this problem. Another problem of TFETs is the superlinear onset and delayed saturation of the output characteristics. It has been shown that a large channel DOS degrades the output characteristics through large channel inversion charge [18], [19]. This is particularly relevant for pTFETs since the valence band DOS of most III-V materials is very large. These two issues make it very challenging to build complementary III-V TFET logic, which requires both high-performance nTFETs and pTFETs. Wu *et al.* [19] note that the required source and channel materials for HJ nTFETs and pTFETs differ greatly.

For HJ nTFETs, it has been previously shown that better ON/OFF ratio is achieved by adopting $(1\bar{1}0)$/[110] as the confinement/transport crystal orientation, because smaller tunnel barrier energy and transport effective masses are found in this orientation [11]. It has been further shown that the ballistic I_{ON} can be greatly increased by adding two more HJs, one in the channel [11] and one in the source, so as to form a 3HJ design [12]. In this paper, we show that by crystal orientation engineering, using the 3HJ design, we can also solve the above mentioned problems of pTFETs,

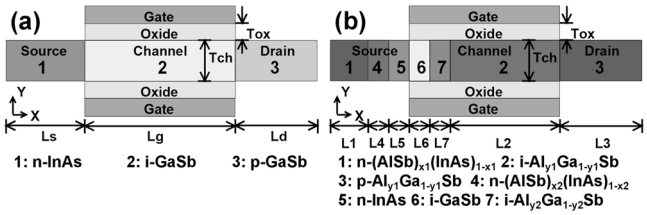

FIGURE 1. **Device structures and material compositions of a HJ pTFET (a) and a 3HJ pTFET (b).**

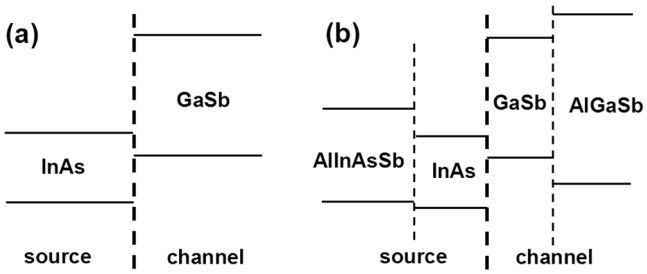

FIGURE 2. **Band alignments of the HJ pTFET (a) and the 3HJ pTFET (b). The transition layers in Fig. 1 (b) are not shown here.**

achieving very large ballistic $I_{\rm ON}$ as well as improved output I-V characteristics.

II. DEVICE STRUCTURES AND SIMULATION METHOD

The ultra-thin-body (UTB) HJ pTFET consists of an InAs source and a GaSb channel/drain (Fig. 1 (a)), with the band alignment shown in Fig. 2 (a) and the device parameters listed in Table 1. Note that heterostructure vertical TFETs have been fabricated and experimentally characterized [20], [21]. The 3HJ pTFET proposed here consists of an $(AlSb)_{x1}(InAs)_{1-x1}$ source, an $(AlSb)_{x2}(InAs)_{1-x2}$ source transition layer, an InAs source well, a GaSb channel well, an $Al_{y2}Ga_{1-y2}Sb$ channel transition layer, and an $Al_{y1}Ga_{1-y1}Sb$ channel/drain (Fig. 1 (b)). The materials are chosen so that they are lattice-matched to each other and they form a band alignment as shown in Fig. 2 (b). For ease of epitaxial growth, other material systems, such as the InP/InAs/GaSb/GaAsSb system with lattice-mismatched materials [22], will be considered in future studies. The mole fractions x1, x2, y1, y2, and the region lengths L4 to L7 are the design parameters to be optimized for the largest $I_{\rm ON}$. An optimal parameter set is given in Table 1 and please note that such parameter set may be non-unique.

The NEMO5 tool [23] is used to simulate the devices by solving Poisson equation and open boundary Schrödinger equation [24] self-consistently. The device Hamiltonian is described by transferrable full-band tight binding (TB) scheme ($sp^3d^5s^*$ basis including spin-orbit coupling) [25], whose parameters at 300K are taken from [26]. We use the virtual crystal approximation [27] to describe the alloys and the TB parameters are linearly interpolated from their corresponding binaries. The oxide (assuming Al_2O_3 here) is treated as an impenetrable potential barrier in the transport equation. As calculated in [28], the InAs-Al_2O_3 valence band offset (VBO) is very large (4.8eV). Assuming the VBO between GaSb (AlSb) and InAs is 0.56eV (0.15eV), the VBO between GaSb (AlSb) and Al_2O_3 will be 5.36eV (4.95eV). A thin GaSb or AlSb channel with 1.8nm thickness considered in the design does not reduce the semiconductor-to-oxide barrier height significantly since the hole quantization energy is <0.5eV. Various scattering effects, such as the electron-phonon scattering, electron-electron scattering beyond Hartree approximation, discrete dopant scattering, alloy scattering, and surface roughness scattering, are not modeled here due to numerical complexity. Some of these scattering phenomena may have non-negligible effects on the device characteristics and we are currently working to model these effects. The dielectric-semiconductor interface trap assisted tunneling and the Shockley-Read-Hall generation-recombination processes, seriously affecting the SS and leakage floor of most TFETs [29], [30], are not considered in this study. These considerations may in part drive the ultimate choice of channel materials in these designs.

TABLE 1. **List of device parameters. *Dx* denotes the doping density of region *x*. ϵ_{ox} is the dielectric constant of the oxide region.**

Ls	Lg	Ld	Tch	Tox	ϵ_{ox}
15nm	15nm/30nm	10nm	1.8nm	1.8nm	9.0
$D1$ ($\rm cm^{-3}$)	$D3$ ($\rm cm^{-3}$)	L4	L5	L6	L7
1×10^{19}	5×10^{19}	2.0nm	3.3nm	1.7nm	2.0nm
$D4$ ($\rm cm^{-3}$)	$D5$ ($\rm cm^{-3}$)	x1	y1	x2	y2
5×10^{19}	5×10^{19}	0.23	1.0	0.12	0.5

III. HETEROJUNCTION (HJ) PTFET

The $(1\bar{1}0)$/[110] orientation performs better than the (001)/[100] orientation at 15nm channel length and 1.8nm channel thickness. As compared in Fig. 3 (a), with $V_{\rm DD}=0.3$V and $I_{\rm OFF}=1{\rm nA}/\mu{\rm m}$, $I_{\rm ON}$ is $14.5\mu{\rm A}/\mu{\rm m}$ in the $(1\bar{1}0)$/[110] orientation. While in the (001)/[100] orientation $I_{\rm ON}$ is only $1.4\mu{\rm A}/\mu{\rm m}$ although the SS is better. The $(1\bar{1}0)$/[110] orientation not only improves $I_{\rm ON}$ but also improves the superlinear onset and delayed saturation of the $I_{\rm DS}$-$V_{\rm DS}$ characteristics. As compared in Fig. 3 (b), the onset and saturation voltages, defined here as the drain voltages corresponding to 10% and 90% of the maximum drain current, are both reduced in the $(1\bar{1}0)$/[110] orientation.

The improvements can be understood from the band diagrams (Fig. 3 (c)) and transmission probabilities (Fig. 3 (d)). Compared with the (001)/[100] orientation, the $(1\bar{1}0)$/[110] orientation has larger transmission below the channel valence band edge (Ev), leading to larger $I_{\rm ON}$. However, its transmission above the channel Ev is also larger and the slope is less steep, leading to larger source-to-drain leakage and larger SS. As seen in the band structures plotted in Fig. 4, the $(1\bar{1}0)$/[110] InAs/GaSb UTB has smaller tunnel barrier energy and transport effective masses than the (001)/[100] InAs/GaSb UTB. Moreover, the source Fermi degeneracy, *i.e.*, the energy separation between the source Fermi level and the conduction band edge (Ec), is larger (due to the smaller conduction band DOS shown in Fig. 5 (a)) and the

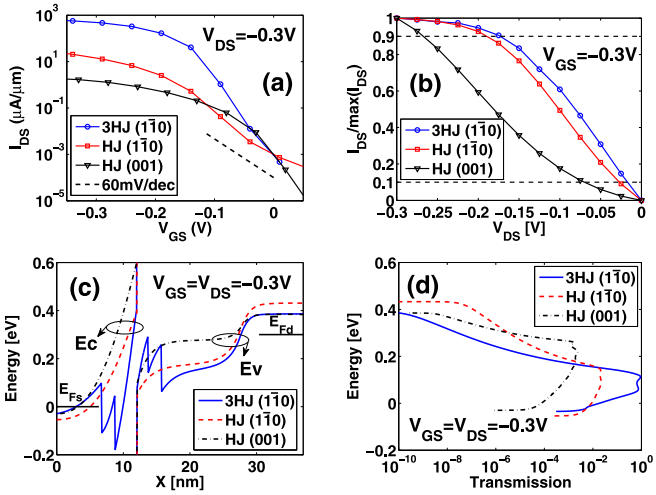

FIGURE 3. **Transfer characteristics (a) and normalized output characteristics (b), after threshold voltage adjustment for the same I_{OFF} = 1nA/μm. Band diagrams (c) and transmission probabilities (d) at ON state. Two HJ pTFETs, in the (001)/[100] and in the (1$\bar{1}$0)/[110] orientation, respectively, and one 3HJ pTFET in the (1$\bar{1}$0)/[110] orientation are compared. Ec (Ev): conduction (valence) band edge. E_{Fs} (E_{Fd}): source (drain) Fermi level.**

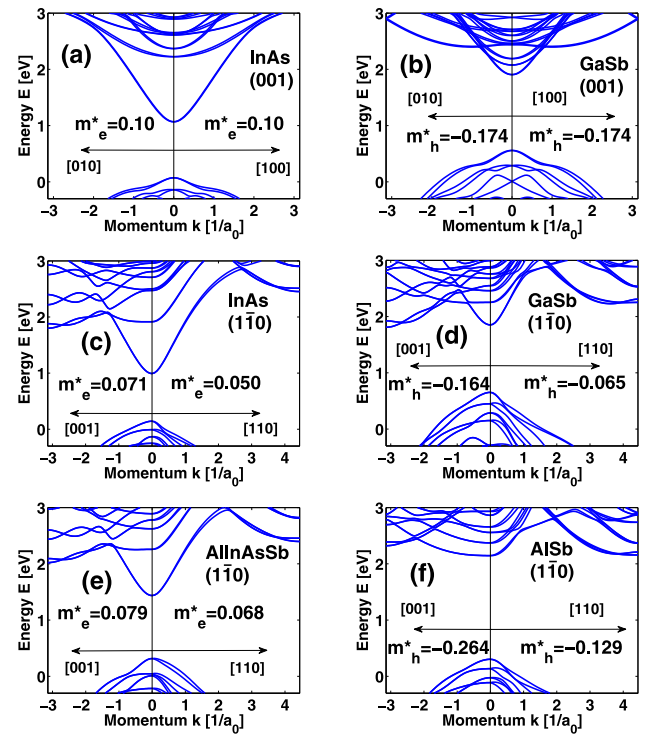

FIGURE 4. ***E-k*** **diagrams for 1.8nm thick UTBs with (001) InAs (a), (001) GaSb (b), (1$\bar{1}$0) InAs (c), (1$\bar{1}$0) GaSb (d), (1$\bar{1}$0) $(AlSb)_{0.23}(InAs)_{0.77}$ (e), and (1$\bar{1}$0) AlSb (f), in the transport direction (positive *k*) and transverse direction (negative *k*). The a_0 is the lattice constant. The m_e^* (m_h^*) is the electron (hole) effective mass at the band edge. Note that the GaSb UTB can be indirect band-gap since the bulk Γ and L valleys have different confinement effective masses [31], [32]; the AlSb UTB is close to direct band-gap due to the folding of the low-energy bulk X valleys [33].**

channel valence band DOS is smaller (Fig. 5 (b)), changes which improve the superlinear onset and reduce the delayed saturation [18], [19], [34].

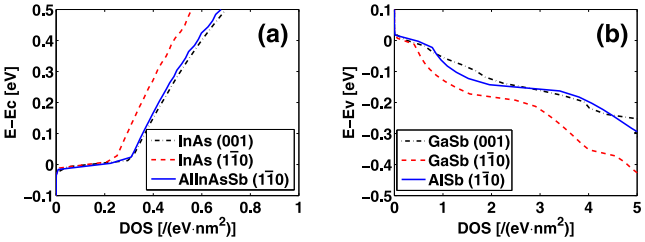

FIGURE 5. **(a) Conduction and (b) valence band DOS of the six UTBs in Fig. 4.**

IV. TRIPLE-HETEROJUNCTION (3HJ) PTFET

The 3HJ design can overcome the shortcomings of the (1$\bar{1}$0)/[110] HJ pTFET, i.e., the degraded SS and the small I_{ON}. Fig. 3 (a) shows that the (1$\bar{1}$0)/[110] 3HJ design greatly improves the SS and I_{ON} of the (1$\bar{1}$0)/[110] HJ design, with 492μA/μm ballistic I_{ON} obtained at V_{DD} = 0.3V and I_{OFF} = 1nA/μm. The reference InAs/GaSb HJ pTFETs show 1.4μA/μm and 14.5μA/μm ballistic I_{ON} respectively in the (001)/[100] and (1$\bar{1}$0)/[110] orientations. Fig. 3 (b) shows that the output I_{DS}-V_{DS} characteristics are improved; comparing the (1$\bar{1}$0)/[110] 3HJ and (001)/[100] HJ designs, the onset (saturation) voltage is reduced from -0.070V (-0.267V) to -0.017V (-0.173V). Fig. 3 (c) and (d) show that the 3HJ design has a much thinner tunnel barrier and thus much larger tunneling probability (approaching unity) when turned on. Further, the 3HJ design shows a much steeper variation of transmission *vs.* energy above the channel Ev, implying less source-to-drain leakage and steeper turn-off characteristics.

From Fig. 4 (c) and (e) it is observed that a (1$\bar{1}$0) AlInAsSb UTB has higher conduction band edge energy than a (1$\bar{1}$0) InAs UTB. This conduction band offset forms a quantum well in the source, which shortens the source depletion length and creates a resonant state above the well, both effects enhancing the tunneling probability. Further, the (1$\bar{1}$0) AlInAsSb UTB has larger electron effective masses (in both transport and transverse directions) than the (1$\bar{1}$0) InAs UTB, thus a larger conduction band DOS (Fig. 5 (a)) and reduced source Fermi degeneracy (Fig. 3 (c)). From Fig. 4 (d) and (f) it is found that the (1$\bar{1}$0) AlSb UTB has lower valence band edge than the (1$\bar{1}$0) GaSb UTB. This valence band offset forms a quantum well in the channel, which also shortens the tunnel barrier thickness and creates another resonant state below the well, both further enhancing the tunneling probability. Moreover, the AlSb UTB channel has larger hole effective masses than the GaSb UTB channel, leading to smaller source-to-drain leakage. Inserting transition layers in the source HJ and channel HJ makes further improvements by further increasing the electric field at the tunnel junction and by tuning the positions of the resonant states. Note that, although the source Fermi degeneracy is reduced and the channel DOS is increased (Fig. 5 (b)), the output characteristic is not degraded. This is due to the much higher transmission transparency enabled by the 3HJ design.

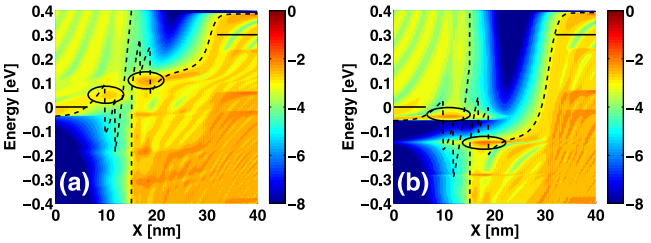

FIGURE 6. **Logarithmic scale LDOS ($k_z = 0$) of the 3HJ pTFET, at ON (a) and OFF (b) states. Band diagrams (dashed lines) and contact Fermi levels (solid lines) are superimposed. The quasi-bound states are highlighted with circles.**

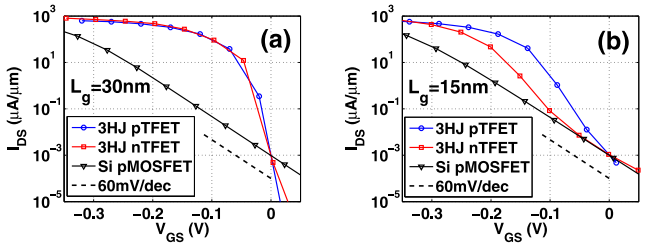

FIGURE 7. **Transfer characteristics of the 3HJ pTFET, in comparison with the 3HJ nTFET (using the same materials and orientations) and Si pMOSFET (with the same dimensions and orientations, the source and drain are p-type doped with density 1×10^{20}cm^{-3}), for $L_g = 30$nm (a) and $L_g = 15$nm (b). $V_{DS} = -0.3$V and the threshold voltages are adjusted for the same $I_{OFF} = 1$nA/μm.**

Fig. 6 (a) and (b) depict the ON and OFF state local density of states (LDOS). In the ON state, the two resonant states created by the two quantum wells both fall in the Fermi conduction window, enhancing the current. In the OFF state, there are no quasi-bound states inside the quantum wells, reducing the thermal emission induced leakage. However, because the tunnel barrier is so thin, evanescent states incident from the source (channel) could still couple to the propagating states of the channel (source) through interaction with phonons and other electrons, forming a leakage current path that is not modeled here. If the device is further scaled to sub-10nm channel lengths, the OFF-state leakage could be dominated by source-to-drain tunneling.

V. DEVICE COMPARISON

Fig. 7 compares the transfer characteristics of the 3HJ pTFETs with corresponding 3HJ nTFETs [12] and Si pMOSFETs for two channel lengths, all from ballistic quantum transport simulations. For $L_g = 30$nm (15nm), the 3HJ pTFET has $I_{ON} = 606\mu$A/μm (492μA/μm), which is comparable to $I_{ON} = 712\mu$A/μm (428μA/μm) of the 3HJ nTFET and much larger than $I_{ON} = 81\mu$A/μm (55μA/μm) of the Si pMOSFET, all measured at $V_{DD} = 0.3$V and $I_{OFF} = 1$nA/μm. For $L_g = 15$nm, the 3HJ pTFET has better SS and thus slightly larger I_{ON} than the 3HJ nTFET, owing to the larger channel band gap and channel effective mass of the 3HJ pTFET.

VI. CONCLUSION

III-V pTFET typically has a low I_{ON}, nonlinear output I-V characteristics, and delayed current saturation. This is because its density of states is small in the source and large in the channel. The triple heterojunction design analysis shows, that by engineering the band gaps, effective masses, and band alignments through proper choice of crystal orientations and material compositions, both very large ballistic I_{ON} and improved output behaviors can be obtained. If the fabrication defects can be controlled, this design would enable a high-performance low-power complementary TFET logic that is built solely with III-V materials. Phonon-assisted tunneling, carrier thermalization in the source, and scattering mechanisms in general, will degrade the 3HJ-TFET's I_{ON} at a specified I_{OFF} and V_{DD}. Detailed studies of these effects will be reported separately.

ACKNOWLEDGMENT

NEMO5 developments were critically supported by an NSF Peta-Apps award OCI-0749140 and by Intel Corp.

REFERENCES

[1] A. M. Ionescu and H. Riel, "Tunnel field-effect transistors as energy-efficient electronic switches," *Nature*, vol. 479, pp. 329–337, Nov. 2011, doi: 10.1038/nature1067.

[2] D. K. Mohata *et al.*, "Demonstration of MOSFET-like on-current performance in arsenide/antimonide tunnel FETs with staggered hetero-junctions for 300mV logic applications," in *Proc. IEEE Int. Electron Devices Meeting (IEDM)*, Washington, DC, USA, Dec. 2011, pp. 33.5.1–33.5.4, doi: 10.1109/IEDM.2011.6131665.

[3] S. Brocard, M. G. Pala, and D. Esseni, "Design options for hetero-junction tunnel FETs with high on current and steep sub-threshold voltage slope," in *Proc. IEEE Int. Electron Devices Meeting (IEDM)*, Washington, DC, USA, Dec. 2013, pp. 5.4.1–5.4.4, doi: 10.1109/IEDM.2013.6724567.

[4] D. Verreck *et al.*, "Uniform strain in heterostructure tunnel field-effect transistors," *IEEE Electron Device Lett.*, vol. 37, no. 3, pp. 337–340, Mar. 2016, doi: 10.1109/LED.2016.2519681.

[5] U. E. Avci and I. A. Young, "Heterojunction TFET scaling and resonant-TFET for steep subthreshold slope at sub-9nm gate-length," in *Proc. IEEE Int. Electron Devices Meeting (IEDM)*, Washington, DC, USA, Dec. 2013, pp. 4.3.1–4.3.4, doi: 10.1109/IEDM.2013.6724559.

[6] M. G. Pala and S. Brocard, "Exploiting hetero-junctions to improve the performance of III–V nanowire tunnel-FETs," *IEEE J. Electron Devices Soc.*, vol. 3, no. 3, pp. 115–121, May 2015, doi: 10.1109/JEDS.2015.2395719.

[7] P. Long *et al.*, "Design and simulation of GaSb/InAs 2D transmission-enhanced tunneling FETs," *IEEE Electron Device Lett.*, vol. 37, no. 1, pp. 107–110, Jan. 2016, doi: 10.1109/LED.2015.2497666.

[8] K. Ganapathi and S. Salahuddin, "Heterojunction vertical band-to-band tunneling transistors for steep subthreshold swing and high on current," *IEEE Electron Device Lett.*, vol. 32, no. 5, pp. 689–691, May 2011, doi: 10.1109/LED.2011.2112753.

[9] S. Brocard, M. G. Pala, and D. Esseni, "Large on-current enhancement in hetero-junction tunnel-FETs via molar fraction grading," *IEEE Electron Device Lett.*, vol. 35, no. 2, pp. 184–186, Feb. 2014, doi: 10.1109/LED.2013.2295884.

[10] W. Li *et al.*, "Polarization-engineered III-nitride heterojunction tunnel field-effect transistors," *IEEE J. Exploratory Solid-State Comput. Devices Circuits*, vol. 1, pp. 28–34, 2015, doi: 10.1109/JXCDC.2015.2426433.

[11] P. Long, J. Z. Huang, M. Povolotskyi, G. Klimeck, and M. J. W. Rodwell, "High-current tunneling FETs with (1$\bar{1}$0) orientation and a channel heterojunction," *IEEE Electron Device Lett.*, vol. 37, no. 3, pp. 345–348, Mar. 2016, doi: 10.1109/LED.2016.2523269.

[12] P. Long *et al.*, "Extremely high simulated ballistic currents in triple-heterojunction tunnel transistors," in *Proc. 74th Annu. Device Res. Conf. (DRC)*, Newark, DE, USA, Jun. 2016, pp. 1–2.

[13] J. Knoch and J. Appenzeller, "Modeling of high-performance p-type III–V heterojunction tunnel FETs," *IEEE Electron Device Lett.*, vol. 31, no. 4, pp. 305–307, Apr. 2010, doi: 10.1109/LED.2010.2041180.
[14] U. E. Avci, R. Rios, K. J. Kuhn, and I. A. Young, "Comparison of power and performance for the TFET and MOSFET and considerations for P-TFET," in *Proc. 11th IEEE Int. Conf. Nanotechnol.*, Portland, OR, USA, Aug. 2011, pp. 869–872, doi: 10.1109/NANO.2011.6144631.
[15] U. E. Avci, D. H. Morris, and I. A. Young, "Tunnel field-effect transistors: Prospects and challenges," *IEEE J. Electron Devices Soc.*, vol. 3, no. 3, pp. 88–95, May 2015, doi: 10.1109/JEDS.2015.2390591.
[16] J. Z. Huang, L. Zhang, P. Long, M. Povolotskyi, and G. Klimeck, "Quantum transport simulation of III-V TFETs with reduced-order **k**·**p** method," in *Tunneling Field Effect Transistor Technology*, L. Zhang and M. Chan, Eds. Cham, Switzerland: Springer, 2016, pp. 151–180. doi: 10.1007/978-3-319-31653-6_6.
[17] D. Verreck *et al.*, "Improved source design for p-type tunnel field-effect transistors: Towards truly complementary logic," *Appl. Phys. Lett.*, vol. 105, no. 24, Dec. 2014, Art. no. 243506, doi: 10.1063/1.4904712.
[18] Y. Taur, J. Wu, and J. Min, "An analytic model for heterojunction tunnel FETs with exponential barrier," *IEEE Trans. Electron Devices*, vol. 62, no. 5, pp. 1399–1404, May 2015, doi: 10.1109/TED.2015.2407695.
[19] C. Wu, R. Huang, Q. Huang, J. Wang, and Y. Wang, "Design guideline for complementary heterostructure tunnel FETs with steep slope and improved output behavior," *IEEE Electron Device Lett.*, vol. 37, no. 1, pp. 20–23, Jan. 2016, doi: 10.1109/LED.2015.2499183.
[20] G. Zhou *et al.*, "Novel gate-recessed vertical InAs/GaSb TFETs with record high I_{ON} of 180$\mu A/\mu m$ at V_{DS}=0.5V," in *Proc. IEEE Int. Electron Devices Meeting (IEDM)*, San Francisco, CA, USA, Dec. 2012, pp. 32.6.1–32.6.4, doi: 10.1109/IEDM.2012.6479154.
[21] E. Lind, E. Memišević, A. W. Dey, and L.-E. Wernersson, "III-V heterostructure nanowire tunnel FETs," *IEEE J. Electron Devices Soc.*, vol. 3, no. 3, pp. 96–102, May 2015, doi: 10.1109/JEDS.2015.2388811.
[22] P. Long *et al.*, "High-current InP-based triple heterojunction tunnel transistors," in *Proc. 28th Int. Conf. Indium Phosphide Related Mater. (IPRM)*, Toyama, Japan, Jun. 2016, pp. 1–2.
[23] S. Steiger, M. Povolotskyi, H.-H. Park, T. Kubis, and G. Klimeck, "NEMO5: A parallel multiscale nanoelectronics modeling tool," *IEEE Trans. Nanotechnol.*, vol. 10, no. 6, pp. 1464–1474, Nov. 2011, doi: 10.1109/TNANO.2011.2166164.
[24] M. Luisier, A. Schenk, W. Fichtner, and G. Klimeck, "Atomistic simulation of nanowires in the $sp^3d^5s^*$ tight-binding formalism: From boundary conditions to strain calculations," *Phys. Rev. B*, vol. 74, no. 20, 2006, Art. no. 205323, doi: 10.1103/PhysRevB.74.205323.
[25] Y. P. Tan, M. Povolotskyi, T. Kubis, T. B. Boykin, and G. Klimeck, "Tight-binding analysis of Si and GaAs ultrathin bodies with subatomic wave-function resolution," *Phys. Rev. B*, vol. 92, no. 8, 2015, Art. no. 085301, doi: 10.1103/PhysRevB.92.085301.
[26] Y. Tan *et al. Tight Binding Parameters by DFT Mapping*. Accessed on Apr. 26, 2016. [Online]. Available: https://nanohub.org/resources/15173
[27] R. Hill, "Energy-gap variations in semiconductor alloys," *J. Phys. C Solid State Phys.*, vol. 7, no. 3, pp. 521–526, 1974. [Online]. Available: http://iopscience.iop.org/0022-3719/7/3/009
[28] J. Robertson and B. Falabretti, "Band offsets of high K gate oxides on III-V semiconductors," *J. Appl. Phys.*, vol. 100, no. 1, pp. 1–8, 2006, doi: 10.1063/1.2213170.
[29] S. Mookerjea, D. Mohata, T. Mayer, V. Narayanan, and S. Datta, "Temperature-dependent I-V characteristics of a vertical $In_{0.53}Ga_{0.47}As$ tunnel FET," *IEEE Electron Device Lett.*, vol. 31, no. 6, pp. 564–566, Jun. 2010, doi: 10.1109/LED.2010.2045631.
[30] U. E. Avci *et al.*, "Study of TFET non-ideality effects for determination of geometry and defect density requirements for sub-60mV/dec Ge TFET," in *Proc. IEEE Int. Electron Devices Meeting (IEDM)*, Washington, DC, USA, Dec. 2015, pp. 34.5.1–34.5.4, doi: 10.1109/IEDM.2015.7409828.
[31] M. Rodwell *et al.*, "III–V FET channel designs for high current densities and thin inversion layers," in *Proc. 68th Annu. Device Res. Conf. (DRC)*, Notre Dame, IN, USA, Jun. 2010, pp. 149–152, doi: 10.1109/DRC.2010.5551882.
[32] S. R. Mehrotra *et al.*, "Simulation study of thin-body ballistic n-MOSFETs involving transport in mixed Γ-L valleys," *IEEE Electron Device Lett.*, vol. 34, no. 9, pp. 1196–1198, Sep. 2013, doi: 10.1109/LED.2013.2273072.
[33] J.-B. Xia and K. W. Cheah, "Quantum confinement effect in silicon quantum-well layers," *Phys. Rev. B*, vol. 56, no. 23, pp. 14925–14928, Dec. 1997, doi: http://dx.doi.org/10.1103/PhysRevB.56.14925
[34] B. Rajamohanan, D. Mohata, A. Ali, and S. Datta, "Insight into the output characteristics of III-V tunneling field effect transistors," *Appl. Phys. Lett.*, vol. 102, Mar. 2013, Art. no. 092105, doi: 10.1063/1.4794536.

JUN Z. HUANG received the B.E. degree from Nankai University in 2004, the M.E. degree from Shanghai Jiao Tong University in 2010, and the Ph.D. degree from the University of Hong Kong in 2013, all in electrical engineering. He researched on compact modeling of carbon nanotube transistors, during the master's degree. He researched on fast numerical algorithms for efficient quantum transport simulations and applied them to study nanoscale metal-oxide-semiconductor transistors and tunnel transistors during the Ph.D. degree. Since 2013, he has been a Post-Doctoral Researcher with the Network for Computational Nanotechnology, Purdue University, where he has been involved in development and applications of Nanoelectronics Modeling software NEMO5.

PENGYU LONG received the B.S. degree in electronic science and technology from the Huazhong University of Science and Technology, China, in 2012, and the M.S. degree in electrical engineering from Purdue University in 2015. He is currently pursuing the Ph.D. degree in electric engineering with Network for Computational Nanotechnology. His current research interests includes modeling electronic transport in steep subthreshold swing transistors for low voltage applications.

MICHAEL POVOLOTSKYI received the Ph.D. degree in electrical engineering from University of Rome "Tor Vergata," Rome, Italy, in 2004. In 2008, he joined the Network for Computational Electronics, Purdue University. His research area is computational electronics. Since the beginning he have been working on simulations of lasers, transistors, memory cells to both advance the technology and create design tools for the engineer community. He was a Post-Doctoral Fellow with Georgia Tech, he contributed into several scientific software packages, such as an open source package nextnano3, primarily developed in the Technical University of Munich, Germany, multiscale finite element package TiberCAD and laser simulator for Canon Inc. He researches on design and development of an atomistic nanoelectronics simulation package NEMO5 with Purdue University. He conducts research in the modeling methodologies such as tight-binding methods, quantum transport, and high performance computing. His current work sponsored by NSF, aims to design a transistor for low power very large scale integration applications.

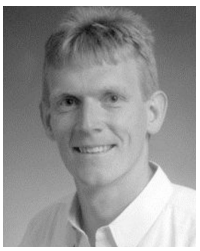

GERHARD KLIMECK (S'91–M'95–SM'04–F'13) received the German Electrical Engineering degree from Ruhr-University Bochum in 1990 and the Ph.D. from Purdue University in 1994. He is the Reilly Director of the Center for Predictive Materials and Devices (c-PRIMED) and Network for Computational Nanotechnology (NCN) and a Professor of the Electrical and Computer Engineering, Purdue University. He leads the development and deployment of Web-based simulation tools, research seminars, tutorials, and classes. He has co-authored 36 tools on nanoHUB that have been used by over 45 000 users. Over 11 000 students used these tools in formalized educational settings such as homework or project assignments in over 776 courses at 64 institutions. His lectures and tutorials have been viewed by over 305 000 nanoHUB users. He was the Technical Group Supervisor for the Applied Cluster Computing Technologies Group, NASA Jet Propulsion Laboratory. He was a Technical Staff Member with the Central Research Laboratory, Texas Instruments. His research interest is in the modeling of nanoelectronic devices, parallel computing, and the study of user behavior and assessment. He has been the lead on the development of NEMO 3-D, a tool that enables the simulation of tens-of-million atom quantum dot systems, and NEMO 1-D, the first nanoelectronic CAD tool. His work is documented in over 470 peer-reviewed publications and over 700 conference presentations. He is also a fellow of the Institute of Physics and the American Physical Society.

MARK J. W. RODWELL (M'89–SM'99–F'03) received the Ph.D. degree from Stanford University, Stanford, CA, USA, in 1988.

He holds the Doluca Family Endowed Chair in Electrical and Computer Engineering with UCSB. He directs the UCSB node of the NSF Nanofabrication Infrastructure Network. His research group develops nm MOSFFETs, THz transistors and mm-wave/THz ICs.

Prof. Rodwell was a recipient of the 2010 IEEE Sarnoff Award, the 2012 IEEE Marconi Prize Paper Award, and the 1997 IEEE Microwave Prize.